

The Far Field Hubble Constant¹

Tod R. Lauer

Kitt Peak National Observatory, National Optical Astronomy Observatories,² P. O. Box 26732, Tucson, AZ 85726
Electronic mail: lauer@noao.edu

John L. Tonry

Institute for Astronomy, University of Hawaii, 2680 Woodlawn Dr., Honolulu, HI 96822
Electronic mail: jt@avidya.ifa.hawaii.edu

Marc Postman³

Space Telescope Science Institute,⁴ 3700 San Martin Dr., Baltimore, MD 21218
Electronic mail: postman@stsci.edu

Edward A. Ajhar

Kitt Peak National Observatory, National Optical Astronomy Observatories,² P. O. Box 26732, Tucson, AZ 85726
Electronic mail: ajhar@noao.edu

and

Jon A. Holtzman

New Mexico State University, Box 30001, Dept. 4500, Las Cruces, NM 88003
Electronic mail: holtz@nmsu.edu

ABSTRACT

We used *HST* to obtain surface brightness fluctuation (SBF) observations of four nearby brightest cluster galaxies (BCG) to calibrate the BCG Hubble diagram of Lauer & Postman (1992). This BCG Hubble diagram contains 114 galaxies covering the full celestial sphere and is volume limited to 15,000 km s⁻¹, providing excellent sampling of the far-field Hubble flow. The SBF zero point is based on the Cepheid calibration of the ground I_{KC} method (Tonry et al. 1997) as extended to the WFPC2 F814W filter by Ajhar et al. (1997). The BCG globular cluster luminosity functions give

¹Based on observations with the NASA/ESA *Hubble Space Telescope*, obtained at the Space Telescope Science Institute (STScI), which is operated by the Association of Universities for Research in Astronomy (AURA), Inc., under National Aeronautics and Space Administration (NASA) Contract NAS 5-26555.

²The National Optical Astronomy Observatories are operated by AURA, Inc., under cooperative agreement with the National Science Foundation.

³Visiting Astronomer Cerro Tololo Inter-American Observatory, NOAO.

⁴STScI is operated by AURA, Inc., under contract to NASA.

distances essentially identical to the SBF results. Using the velocities and SBF distances of the four BCG alone gives $H_0 = 82 \pm 8 \text{ km s}^{-1} \text{ Mpc}^{-1}$ in the CMB frame, valid on $\sim 4,500 \text{ km s}^{-1}$ scales. Use of BCG as photometric redshift estimators allows the BCG Hubble diagram to be calibrated independently of recession velocities, yielding a far-field $H_0 = 89 \pm 10 \text{ km s}^{-1} \text{ Mpc}^{-1}$ with an effective depth of $\sim 11,000 \text{ km s}^{-1}$. The error in this case is dominated by the photometric cosmic scatter in using BCG as distance estimators. The concordance of the present results with other recent H_0 determinations, and a review of theoretical treatments on perturbations in the near-field Hubble flow, argue that going to the far-field removes an important source of uncertainty, but that there is not a large systematic error to be corrected for to begin with. Further improvements in H_0 depend more on understanding nearby calibrators than on improved sampling of the distant flow.

Subject headings: distance scale — galaxies: distances and redshifts

1. Introduction

A key part of measuring the Hubble constant, H_0 , is to look out far enough so that the bulk velocities of galaxies are trivial compared to the Hubble flow itself. Due to the Virgo cluster infall pattern, observation of the unbiased Hubble flow can only be contemplated at distances in excess of $\sim 3000 \text{ km s}^{-1}$. Furthermore, bulk flows on even larger scales, such as those associated with the Great Attractor, may bias measurement of H_0 . Turner, Cen, & Ostriker (1992) and Shi, Widrow, & Dursi (1996), for example, show that under standard theories of structure formation, measurements of H_0 can depart significantly from its true “global” value due to the inhomogeneous distribution of matter in the universe, unless care is taken to sample deeply with large angular coverage. Indeed, a common concern with many recent H_0 determinations is that they are not truly sampling the distant Hubble flow (Bartlett et al. 1995).

Characterizing the far-field requires observing large numbers of objects at large distances so that the Hubble diagrams are insensitive to random peculiar velocities or bulk flows. Hubble diagrams at present are largely based on the Tully-Fisher or $D_n - \sigma$ relationships, the luminosities of supernovae (SN Ia or SN II), and brightest cluster galaxies (BCG). Tully-Fisher distances are available out to $\sim 9,000 \text{ km s}^{-1}$, and have been recently used to measure a far-field H_0 (Giovanelli et al, 1997), while $D_n - \sigma$ have full-sky coverage out to only $\sim 6,000 \text{ km s}^{-1}$. Only a few SN II have been observed in sufficient detail at large distances (Schmidt et al. 1994), but the SNIa Hubble diagram is becoming richer with time and provides some sampling of the Hubble flow out to $\sim 30,000 \text{ km s}^{-1}$ (Riess, Press, & Kirshner 1996; Hamuy et al. 1996). At present, however, calibration of the SNIa distance scale remains controversial (see Sandage et al. 1996), and the SN Ia diagrams remain relatively sparse at large distances. In this work we focus on calibrating the BCG Hubble diagram, which is based on a recent characterization of BCG as relative distance estimators (Postman & Lauer 1995).

In the classic work of Sandage (1972) and Sandage & Hardy (1973), BCG were used to show that the Hubble flow was linear over a large range in redshift. Lauer & Postman (1994) observed BCG to define a frame for measuring the peculiar velocity of the Local Group, but as this work was in progress they realized that they could test for H_0 variations with distance

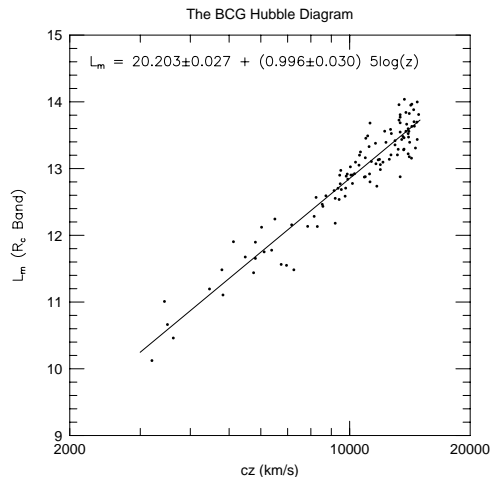


Fig. 1.— The BCG Hubble diagram. R-band metric luminosities of the BCG, corrected by the $L_m - \alpha$ relationship, are plotted as a function of velocity in the Local Group frame. The line is the mean Hubble relation fitted.

with greater precision than was previously available in response to the concerns of Turner, Cen, & Ostriker (1992). Lauer & Postman (1992) presented a Hubble diagram based on the 114 BCG that defined the volume-limited full-sky sample of Abell clusters within $15,000 \text{ km s}^{-1}$, which is shown again here in Figure 1. In brief, the absolute magnitudes of BCG, L_m , measured in apertures of fixed metric size, r_m , can be predicted from $\alpha \equiv d \log L_m / d \log r |_{r_m}$ (Hoesel 1980). Figure 1 shows the metric luminosities as apparent fluxes, corrected by the $L_m - \alpha$ relationship to a standard value of $\alpha = 0.5$.

The BCG Hubble diagram slope is 0.996 ± 0.030 of the expected value, consistent with a uniform Hubble flow over $0.01 \leq z \leq 0.05$. Lauer & Postman (1992) limit any variation in the *apparent* or local H_0 (the Hubble constant measured over a limited depth) as compared to H_0 measured globally over the entire volume, to $\delta_H \equiv \Delta H_0 / H_0 < 0.07$. The SNIa Hubble

diagram also shows no evidence for H_0 variations with distance; Riess, Press, & Kirshner (1996) show its slope (relative to Euclidean) to be 1.005 ± 0.018 . The full-sky coverage of the Abell cluster sample is crucial, as any dipole pattern caused by large bulk flows (such as that advanced by Lauer & Postman 1994) will integrate out of the Hubble diagram to first order. The linearity of the BCG Hubble diagram shows that an excellent estimate of the far-field H_0 can be obtained once the zero point of the diagram is calibrated. We note that BCG presently provide the only volume-limited sample that explores the Hubble flow at these distances.

A Hubble constant can be obtained from the BCG Hubble diagram once an absolute distance is known to a subset of the galaxies. In essence, one transfers the full sample to a common distance, and finds the average absolute luminosity of the BCG on the assumption that the calibrating set is typical. Random velocities and bulk flows of the BCG contribute to the “cosmic scatter” in their luminosity distribution, but cause no systematic offset (with the caveats discussed in §4.2). We contrast this approach to others that use the apparent distance ratio between the Virgo and Coma clusters, or any other near and far aggregate of galaxies, to reach the far-field. Instead, we are using the BCG as complete probes of the Hubble flow over a large volume.

We chose to calibrate the BCG Hubble diagram with surface brightness fluctuation (SBF) distance estimates to four of the nearest BCG. The SBF method (Tonry & Schneider 1988) uses the ratio of the second to first moments of the stellar luminosity function within early-type stellar systems as a distance estimator. The ratio of moments corresponds to an apparent magnitude, \overline{m} , that in the near-IR corresponds to the brightness of a typical red giant star. When the images are deep enough such that a star of apparent luminosity \overline{m} contributes more than a single photon to an observation, the random spatial point-to-point surface brightness fluctuations in a galaxy image are dominated by the finite number of stars it comprises, rather than photon shot noise. A power spectrum of the SBF pattern provides \overline{m} . Use of the SBF method on galaxies with distances known from other methods (see Jacoby et al. 1992 for additional details) provides the zero point \overline{M} , allowing absolute distances to be computed from \overline{m} .

The most recent calibration of the SBF method is presented by Tonry et al. (1997). Major compo-

nents of this work are: 1) understanding how \overline{M} varies with stellar population, 2) determining the zero point of the method, and 3) establishing the universality of the calibration. Tonry et al. observe in the I_{KC} band, which minimizes variations in $\overline{M}_{I_{KC}}$ with stellar population *ab initio*. They also show that variations in $\overline{M}_{I_{KC}}$ are fully characterized by the $(V - I)$ colors of the stellar systems. Based on 149 nearby galaxies they find

$$\overline{M}_{I_{KC}} = (-1.74 \pm 0.07) + (4.5 \pm 0.25)[(V - I)_0 - 1.15]. \quad (1)$$

This relationship has scatter of only 0.05 mag and agrees well with the theoretical calculations of Worthey (1993a, 1993b) both in slope *and* zero point. Tammann (1992) was concerned that an earlier SBF calibration based on $(V - I)$ was incomplete and that $\overline{M}_{I_{KC}}$ additionally depended on the galaxies’ Mg_2 indices. In response, Tonry et al. use their extensive sample to show that there is no correlation between the residuals of equation (1) and Mg_2 . The zero point of equation (1) is based on Cepheid distances to seven spiral galaxies with bulge SBF observations. Tonry et al. present numerous comparisons of SBF to PNLF, Tully-Fisher, $D_N - \sigma$, SNIa, and SN II distances, finding no evidence for any systematic offset between SBF bulge and elliptical galaxy measurements, nor any other systematic effect that challenges the calibration.

Although the nearest BCG are too far away for the SBF method to work from the ground, the high spatial resolution of *HST* allows SBF to be used beyond the 15,000 km s⁻¹ depth of the Lauer & Postman (1994) sample. An important caveat is that there is no direct match to the I_{KC} filter among the WFPC2 filter set. The F814W filter is a close analogue to I_{KC} (see Holtzman et al. 1995a), but requires additional calibration to tie it to the Tonry et al. (1997) zero point. Ajhar et al. (1997) accomplished this task in preparation for the present work, by comparing *HST* F814W SBF observations to the I_{KC} results for 16 galaxies in the Tonry et al. sample. For the WFPC2 CCDs and F814W filter, Ajhar et al. find

$$\overline{M}_{I_{814}} = (-1.73 \pm 0.07) + (6.5 \pm 0.7)[(V - I)_0 - 1.15], \quad (2)$$

with scatter similar to that about equation (1). A key difference between equation (1) and (2) is the steeper relationship between $\overline{M}_{I_{814}}$ and $(V - I)$, which Ajhar et al. show is consistent with the differences between the F814W and I_{KC} filters. Calibration of *HST* for

SBF work is thus crucial for the present work.

2. Observations and Reductions

2.1. BCG Sample Selection

We selected the BCG in four Abell clusters, A262, A3560, A3565, and A3742 for observation. These are among the nearest of the Lauer & Postman (1994) sample so as to minimize *HST* exposure time. We also wanted to minimize the effects of bulk flows on placement of the calibrating BCG within the Hubble diagram, so we selected BCG positioned such that their mean photometric offset about the Hubble line in Figure 1 is largely insensitive to whether the Hubble diagram is constructed from velocities referenced to the cosmic microwave background (CMB), Local Group (LG), or the Abell Cluster (AC) frame solution of Lauer & Postman (1994). Figure 2 shows how the positions of the BCG in the Hubble diagram change with changing velocity system. Complete frame invariance of the results is difficult to achieve with only four BCG, however; we discuss this issue later where our results are affected by it.

The BCG properties are given in Table 1. Photometry, details of BCG identification, and so on are discussed by Postman & Lauer (1995). Velocities are given in the CMB, LG, and AC frames (see Lauer & Postman 1994). The velocities are a weighted average of all galaxies selected to be within the given Abell cluster; the estimated velocity error is 184 km s^{-1} (see Postman & Lauer 1995). Extinctions are from Burstein & Heiles (1984).

2.2. *HST* Observations and Reductions

Images were obtained in WFPC2 using the F814W filter. The galaxies were centered in the high-resolution PC1 chip. While suitable data were obtained in the flanking WFC CCDs, we chose to analyze the PC data only, given its superior resolution, and the greater brightness of the central portions of the BCG with respect to the sky. At the BCG distances, the apparent luminosity of an F814W SBF “star,” \bar{I}_{814} , is extremely faint, thus long exposures are required; the total exposures are given in Table 1. Although our ideal criterion is to obtain at least five photons per \bar{I}_{814} star, our data contained only 2.3–3.8 photons per \bar{I}_{814} . The reasons for the shortfall were 1) *HST* was 5% less sensitive through F814W than prelaunch numbers suggested, 2) the galaxies were about 5% more distant than we had guessed from their redshifts,

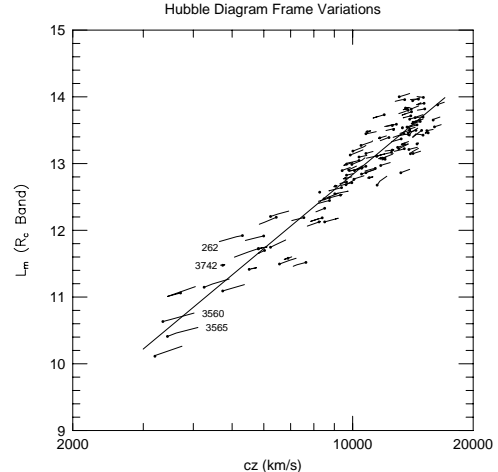


Fig. 2.— The BCG Hubble diagram with frame variations. This figure shows how the BCG move within the Hubble diagram as the velocity frame changes. The lines start at the positions of the BCG in the CMB frame, move through the Local Group frame, ending with the solid points in the Abell Cluster frame. The four BCG with SBF distances are labeled.

and 3) $\bar{M}_{I_{814}}$ was significantly fainter (0.65 mag in the case of A262) because the galaxies were redder than anticipated and \bar{I}_{814} was more sensitive to color than our assumptions. Nevertheless, all four galaxies yielded a strong SBF signal that could be accurately determined.

Because compact artifacts can strongly affect the SBF power spectrum, we built the total exposures from sets of “dithered” half-orbit images to eliminate hot-pixels, CCD defects, as well as cosmic-ray hits. Each individual exposure was typically 1200s long, with the actual exposure time set to maximize the total exposure obtained with two roughly equal exposures per orbit. The dither pattern consisted of moving the telescope between exposures in a skewed-square-spiral pattern, designed to achieve integral-pixel shifts in the WFC CCDs. The pattern opti-

TABLE 1
BCG GALAXY SAMPLE AND OBSERVATIONS

Abell	J2000.0		V_{CMB}	V_{LG}	V_{AC}	E_{B-V}	Date	Time
	RA	DEC	km s ⁻¹	km s ⁻¹	km s ⁻¹			s
262	01 52 46.3	+36 09 05	4650	5130	5310	0.060	96/02/11	16,400
3560	13 31 53.3	-33 14 04	4020	3510	3360	0.038	96/01/16	9,200
3565	13 36 39.1	-33 57 57	4110	3630	3450	0.030	96/01/19	11,600
3742	21 07 52.3	-47 10 43	4680	4800	4740	0.018	96/04/22	16,500

NOTE.—Velocities are weighted averages of all available cluster data given in the Cosmic Microwave Background (CMB), Local Group at rest (LG), or Abell Cluster (AC) frames (see Lauer & Postman 1994 and Postman & Lauer 1995). E_{B-V} values are from Burstein & Heiles (1984). The last two columns are date of the *HST* observations and total exposure time.

mized removal of fixed-pattern CCD defects, while preserving the exact shape of any SBF pattern from exposure to exposure. While one might argue for an approach that would instead optimize information recovered with sub-pixel stepping, we did not have the exposure time available to obtain an equal number of the required 2×2 0.5-pixel steps and were concerned with the effects on the SBF pattern from any *ad hoc* interpolation scheme that might be required to assemble the completed image from a random set of offsets. Ironically, we did not use the WFC images in the present analysis, given the excellent quality and superior resolution of the PC1 images; however, this was a decision made after the data were in hand.

In the dither pattern, each exposure would be shifted from the previous one, by ~ 10 WFC pixels ($\sim 1''$) in either the row or column direction, spiraling around the original pointing, with the exact shift adjusted by ± 1 WFC pixel to avoid having any object land on the same row or column that it may have fallen on in a previous exposure. This latter criterion also meant that the exposure was simultaneously stepped ± 1 pixel in a direction perpendicular to the major step, resulting in the spiral being skewed from perfect alignment with WFC row and column axes. The detailed shifts in all cases reflected the slight misalignment of the WFC CCDs with respect to perfect quadrature with the *HST* sky axes (see Holtzman et al. 1995b).

Fig. 3.— The 710×711 pixel ($\approx 32''$) portion of the PC1 image centered on the BCG in Abell 262. The central portion of the montage shows the galaxy and its central dust clouds; this region is masked from the SBF analysis. The remainder shows the residual after the galaxy model is subtracted (with $8\times$ deeper stretch); most of the objects seen are globular clusters. Some dust is still visible and this is also masked for the SBF analysis.

Integral pixel offsets for the WFC produce non-integral steps in PC1, but for F814W, the PC1 images are nearly Nyquist-sampled, so shifting the images to a common center may be done with little error. As it is, however, we chose to stack the PC1 images with centering only to the nearest pixel to avoid the complexity of patching in the defects prior to interpolation. While this produces a slight blurring at the one-pixel scale, this has little effect on measurement of the SBF signal, because the final composite image remains photon shot-noise limited at the highest-spatial frequencies. This can be simply understood by considering the enclosed energy curve of the PSF. Holtzman et al. (1995b) show that only 32% of the light within the F814W PSF falls within its central core, corresponding to only a single photon for the typical exposure time in the present work.

The final composite PC1 images were assembled

Fig. 4.— The 771×781 pixel ($\approx 34''$) portion of the PC1 image centered on the BCG in Abell 3560. The central portion of the montage shows the galaxy and its central dust ring; this region is masked from the SBF analysis. The remainder shows the residual after the galaxy model is subtracted (with $40\times$ deeper stretch); most of the objects seen are globular clusters.

Fig. 5.— The 791×742 pixel ($\approx 33''$) portion of the PC1 image centered on the BCG in Abell 3565. The central portion of the montage shows the galaxy and its central dust lane; this region is masked from the SBF analysis. The remainder shows the residual after the galaxy model is subtracted (with $60\times$ deeper stretch); most of the objects seen are globular clusters.

Fig. 6.— The 766×766 pixel ($\approx 33''$) portion of the PC1 image centered on the BCG in Abell 3742. No dust was seen in this image, so only the very central portions were excluded from SBF analysis. The concentration of globular clusters around the galaxy is evident.

with an algorithm that looks at the statistical properties of the data set at any pixel location, and rejects extreme values as might be caused by cosmic ray hits or hot pixels. The BCG images are shown in Figures 3 to 6, with the galaxies themselves largely subtracted to emphasize fine detail. Globular clusters are readily visible into the centers of all images. This is the strength of using *HST* for SBF work — globulars, background galaxies, and dust clouds are easily recognized and excluded when measuring the SBF power spectrum. Dust clouds are also visible in three galaxies, A262, A3560, and A3565; indeed, their centers are completely or nearly obscured by dust.

Although SBF are measured from the PC1 images, we do need the WFC images to measure the sky levels, which are required as part of the analysis. Sky levels were measured from a $20'' \times 20''$ patch extracted from the far corner of WF3. This is the corner of WF3 diagonally opposite the WFPC2 vertex, and is thus the portion of the WFPC2 field most distant from the BCG centers; the typical displacement of the sky patch from the galaxy centers is $\sim 125''$. The galaxies still contribute light to the sky measurements at

this modest distance; however, their contribution to the sky is readily estimated and corrected for using ground-based surface photometry extending to much larger radii. The sky values given in Table 2 have been corrected for galaxy light contributions.

2.3. $(V - I)$ Colors

As equation (2) shows, the $\overline{M}_{I_{814}}$ value for a given BCG depends strongly on its $(V - I)$ color. We measure $(V - I)$ from ground-based photometry over an annulus between $5''$ and $15''$ in radius from the galaxy centers to match the area of the PC1 field used for the SBF measurements. The photometry for the three southern BCG was obtained under excellent conditions at the CTIO 1.5m telescope. For A262, the I_{KC} image was obtained at the KPNO 4m, and John Blakeslee kindly obtained the V image at the MDM 2.4m. For the small redshifts of the BCG, the K -corrections are $K_V \approx 2.0z$, and $K_I \approx 1.1z$; galactic absorption corrections are $A_V : A_I : E(B - V) = 3.04 : 1.88 : 1.00$. The observed $(V - I)$, and reduced $(V - I)_0$ colors are both given in Table 2. In passing, we note that ground $(V - I_{KC})$ and WFPC2 $(V_{F555W} - I_{F814W})$ are essentially identical (Holtzman et al. 1995a). While we did not obtain WFPC2 $F555W$ data, we did compare the $F814W$ photometry to the ground I_{KC} data. For $(V - I) \sim 1.25$, Holtzman et al. (1995a) find $I_{KC} - I_{F814W} \approx -0.04$; unfortunately, even with this transformation, the WFPC2 I_{F814W} fluxes are still brighter than the ground values by 0.04 mag with a spread of 0.05 mag. Ajhar et al. (1997) found excellent agreement between WFPC2 I_{F814W} and ground I_{KC} transformed to I_{F814W} for their sample, so the present mismatch is disappointing. Since to first order, we might expect any deviations in ground V to correlate with those in I_{KC} , we chose to base $(V - I)_0$ entirely on ground photometry rather than ground V and WFPC2 $F814W$.

2.4. Measurement of \overline{I}_{814}

Measurement of the fluctuation signal was straightforward, following the steps detailed in Tonry et al. (1997) and Ajhar et al. (1997). Once the PC images were cleaned of cosmic rays and stacked, we subtracted sky; fitted elliptical profiles to the galaxy light; generated and subtracted a synthetic galaxy; ran DoPhot (Schechter et al. 1993) to detect stars, globular clusters, and background galaxies; determined a luminosity function of these objects and created a mask for removing objects brighter than a com-

TABLE 2
SBF MEASURES AND GALAXY DISTANCES

Abell	\bar{I}_{814}	e^-	Sky	$(V-I)$	$(V-I)_0$	$\bar{M}_{I_{814}}$	$(m-M)$	\pm	GCLF
262	33.35 ± 0.15	2.3	21.40	1.401	1.317	-0.642	33.77	0.19	25.85
3560	32.33 ± 0.10	3.4	21.61	1.289	1.234	-1.183	33.35	0.14	25.12
3565	32.47 ± 0.08	3.8	21.70	1.286	1.239	-1.151	33.47	0.13	25.72
3742	33.08 ± 0.08	3.0	21.73	1.305	1.270	-0.950	33.88	0.12	25.77

NOTE.—SBF amplitudes are given as \bar{I}_{814} magnitudes with no reddening or k-corrections, or as number of e^- detected. Sky is I_{814} magnitudes per square arcsecond, after correction for galaxy-light contamination. Colors are $(V-I)$ observed and $(V-I)_0$ after reddening and k-corrections. $\bar{M}_{I_{814}}$ is the predicted SBF absolute luminosity calculated from equation (2). GCLF is the I_{814} turnover magnitude of the globular cluster luminosity function.

pletteness cutoff; and then performed the fluctuation analysis. The basic step in measuring fluctuations is to model the object’s power spectrum as

$$P(k) = P_0 \times E(k) + P_1, \quad (3)$$

where P_1 is a constant giving the background level, and P_0 is another constant used to scale the power spectrum of the PSF, $E(k)$. (Properly speaking, $E(k)$ is an expectation power spectrum that incorporates the galaxy profile and the mask that has been applied to the data.)

There are several sources of uncertainty in deriving the fluctuation power. The first is the normalization and match of the PSF to the data. The second arises in fitting the power spectrum: the lowest wavenumbers are always corrupted, but there is no fluctuation signal at high wavenumbers, so the choice of precisely which wavenumbers to fit introduces uncertainty. Finally, the raw P_0 variance is corrected for the variance from residual, undetected point sources, and this correction also carries an error.

We used the same PSF as Ajhar et al. (1997), which was constructed from several F814W star images obtained in 1995. The wings of the PSF were provided by archive exposures of stars centered in PC1 to provide routine monitoring of the F814W filter zero point calibration. The core of the PSF was constructed from four PC1 images of the quadrupole gravitational lens 2237+0305, which were dithered in

a 2×2 pattern of 0.5 PC pixel steps. This data set allowed the core to be recovered with “perfect” centering on a PC pixel. The composite PSF has a total exposure of 5.8×10^5 photons. It is an excellent match to the observed power spectra of the galaxies with the highest signal to noise, A3560 and A3565, over the wavenumbers where SBF dominates, so we deemed it to be suitable for all our observations.

We performed experiments with synthetic PSF images (created by software developed by JAH) with calibrated amounts of defocus and miscentering. We found that the results are completely insensitive to where the PSF was centered, but that P_0 became larger as the PSF became defocussed, as would be expected from its more compact power spectrum. Using a PSF from the extreme secondary displacement caused by “breathing” of the OTA quoted by STScI, we found that \bar{m} brightened by about 0.3 mag. A synthetic PSF with perfect focus gave nearly the same results as the observed PSF, but was still about 0.1 mag brighter, revealing a bit *less* high wavenumber power than the observed PSF. Ajhar et al. also demonstrate that the observed PSF will give very consistent results applied to a variety of observations, and indeed, we are working differentially with respect to those results anyway. We thus conclude that the observed PSF is appropriate to use for the fluctuation analysis, with mismatch and normalization error amounting to about 0.05 mag.

Power Spectra

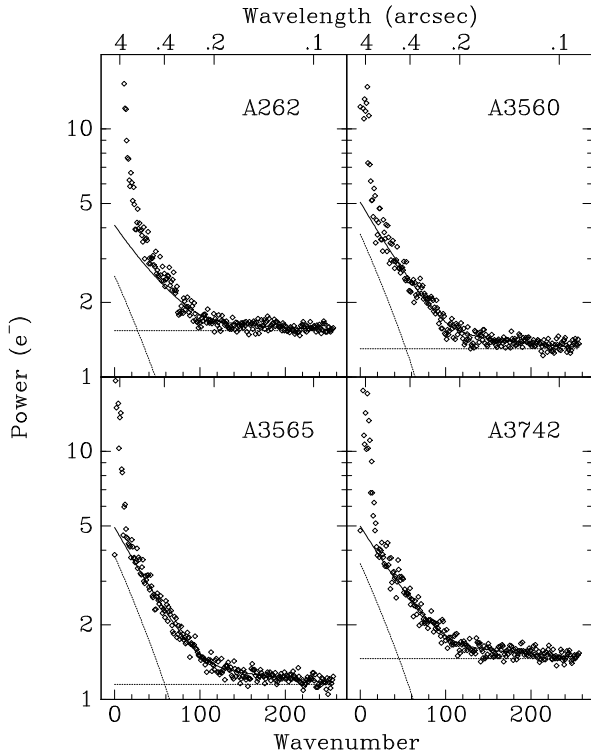


Fig. 7.— The power spectra of each galaxy in the annulus with radii 5''–8–11''–7. The dotted lines show the components of white noise power and PSF power. The solid lines show the sum of the fitted power spectra. The diamonds are the azimuthal averages of the data power spectra. The bottom axes indicate wavenumber; the top axes indicate wavelength.

An observed power spectrum always has excess power at wavenumbers below 10 or so (wavelengths longer than ~ 30 pixels), arising from poor flattening, poor galaxy subtraction, dust, etc. With the exception of A262 we found very good agreement with the PSF beyond these contaminated wavenumbers. We normally use the rms variation in P_0 as a function of where we begin the power spectrum fit as an additional error component. In the case of A262 there is a range of P_0 values that are allowed by the power spectrum; this range is reflected in the larger error budget for this galaxy. PSF fits to the power spectra of the BCG are shown in Figure 7.

The contribution from the residual point sources was small — always less than a 0.20 mag correction

to P_0 , and more typically 0.10 mag. Since we think we know this variance contribution quite well, at least to 25%, the contributed error is small. As a test of this, we routinely analyze different annuli independently, and except for A262 we used 4 annuli at 1, 2, 4, and 8'' mean radius (the central annulus was obscured by dust for A262). If we have an error in the residual point source correction (or an unknown source of variance which does not scale with galaxy brightness) it will show up as a radial gradient in \bar{m} . A3560 had a gradient of about 0.1 mag in each of the outer annuli, but the other three had no gradient at the 0.05 mag level, giving us confidence that we have modeled the residual variance well and we have no unforeseen source of variance. The gradient in A3560 may very well be real; there is a 0.04 mag color gradient in $B - R$ from the center to 20'' in radius, which would produce a gradient in \bar{m} consistent with what we see.

The estimates and errors for \bar{m} are derived from the averages of the values determined for each annulus, and the formal uncertainty in the P_0 fitting procedure added in quadrature to 0.05 magnitude for the PSF uncertainty. With the exception of A3560, where we think we see a real gradient in \bar{m} , the scatter between the different annuli is consistent with the error estimates. We list the apparent SBF \bar{I}_{814} fluxes in Table 2 uncorrected for extinction and prior to k-correction. The SBF signal strength in electrons is also given. A262 has the weakest SBF signal, which is reflected in its larger error bars.

2.5. The Turnover of the Globular Cluster Luminosity Function

As discussed above, measuring \bar{m} requires characterization of the galaxy's globular cluster luminosity function (GCLF) to estimate the residual variance contributed by the undetected (faint) portion of the GCLF as well as by the undetected faint galaxies. Figure 8 shows the luminosity functions of the objects found in the images of our sample along with the GCLF, background galaxy, and combined luminosity function fits. The fitting procedure naturally produces an estimate of the GCLF turnover magnitude in the I band for an assumed Gaussian σ width of 1.4 mag. The m_I^0 GCLF turnover magnitudes are listed in Table 2. The estimated turnovers are all near the $I \sim 25$ completeness limit and are uncertain by 0.2–0.3 mag.

Based on the SBF distance moduli, the mean ab-

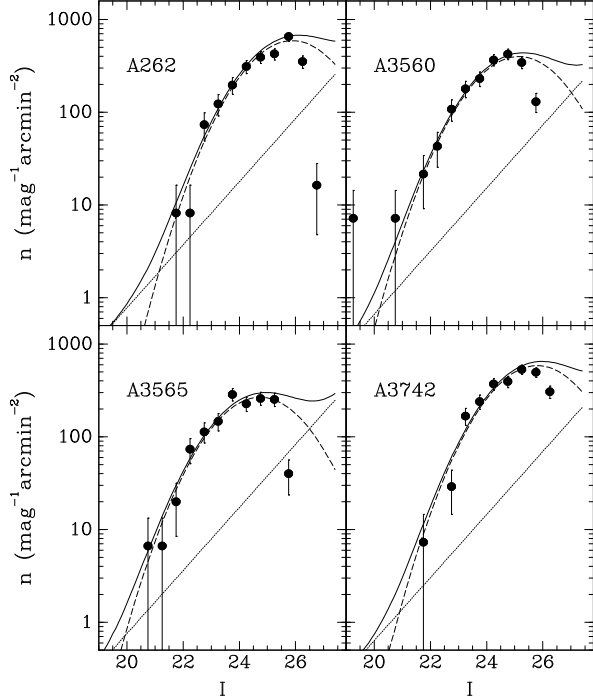


Fig. 8.— The fitted GCLFs and background galaxy luminosity functions. The dashed lines are the GCLFs; dotted lines are the background galaxies. The solid lines are the combined luminosity functions from which the residual variance is computed. The error bars only represent the Poisson scatter in each bin. The radial ranges shown are $3''.0 < r < 21''.4$, $1''.5 < r < 22''.5$, $2''.1 < r < 23''.5$, and $0''.9 < r < 22''.1$ for A262, A3560, A3565, and A3742, respectively.

solute magnitude of the four BCG GCLF turnovers in the I band $\langle M_I^0 \rangle = -8.29 \pm 0.18$; the error is consistent with the measurement errors and an estimated intrinsic scatter in the GCLF technique of ~ 0.25 mag. Few deep I -band GCLFs of giant elliptical galaxies have been published for comparison; however, $\langle M_I^0 \rangle$ is consistent with the M87 measurements of Whitmore *et al.* (1995), who found $m_{I,M87}^0 = 22.67$. Using the SBF distance modulus to the Virgo cluster of 31.03 ± 0.05 (Tonry *et al.* 1997) yields $M_{I,M87}^0 = -8.36$. For additional comparison, a crude estimate of M_I^0 can be based on the following assumptions: 1) Combining the distance modulus to Virgo with the average observed

apparent magnitude for the GCLF turnover in Virgo in the V band of $m_V^0 = 23.75 \pm 0.05$ (Blakeslee & Tonry 1996) yields $M_V^0 = -7.28 \pm 0.07$. 2) Taking the mean color $(V-I)_0 = 1.10 \pm 0.1$, based on the average of the mean $(V-I)_0$ found in Coma's IC 4051 of $(V-I)_0 = 1.08$ (Baum *et al.* 1997) and that found in M87 of $(V-I)_0 = 1.12$ (Whitmore *et al.* 1995) and applying an uncertainty of 0.1 mag, yields an estimate of $M_I^0 = -7.28 - 1.10 = -8.38 \pm 0.12$, also in good agreement with the BCG value.

3. Measurement of H_0

The present data set permits two separate approaches to measuring H_0 . The first and most obvious approach is simply to form Hubble ratios for the four BCG and average them in an optimal way. The BCG all have velocities in excess of $4,000 \text{ km s}^{-1}$ (in the CMB frame), and may be far enough away so that their average Hubble ratio might be close to the true value of H_0 . At the same time, this approach does not make use of the BCG Hubble diagram, nor does it transfer the results to the $15,000 \text{ km s}^{-1}$ far-field. The BCG instead are simply treated as test particles, without reference to their photometric properties (although we do use cluster averages for the velocities).

The second approach is to use the BCG as distance estimators to avoid any use of the velocities of the four SBF BCG themselves, in an effort to skip over the near velocity field — this is the approach promised by the title of our paper. The frame independence of both the BCG Hubble diagram and $L_m - \alpha$ relationship argues that we can successfully reduce the BCG to a common distance. The SBF distances then permit calibration of the BCG as absolute rather than relative distance estimators.

In either approach, the mathematical formalism used to derive a Hubble ratio is the same. For each SBF observation, we compute a distance measurement in Mpc, D , from the expression

$$D = dex(0.2(\bar{I}_{814} - \bar{M}_{I_{814}} - 25)) \quad (4)$$

where \bar{I}_{814} and $\bar{M}_{I_{814}}$ are corrected for extinction and k-dimming. The Hubble ratio is then just

$$H_0 = v/D \quad (5)$$

where v is either the observed velocity of the BCG in the appropriate reference frame (for the first approach) or the estimated velocity of the BCG using the prescription in Postman & Lauer (1995) and summarized in §3.2 (for the second approach).

3.1. H_0 from the SBF BCG Hubble Ratios Alone

The BCG $(V - I)_0$ colors and the F814W SBF calibration of equation 2 allow us to predict the absolute fluctuation magnitude $\overline{M}_{I_{814}}$. Using a \overline{I}_{814} k-correction of $\approx 7z$ (Tonry et al. 1997) and our measured values for the apparent \overline{I}_{814} , we derive the distance moduli and errors listed in Table 2. Converting these to distances in Mpc (equation 4) and using the velocities in the CMB, LG, and AC frames, we compute Hubble ratios in Table 3. The errors listed here include the estimated velocity error of 184 km s^{-1} plus a nominal 100 km s^{-1} allowance for peculiar velocity with respect to the local velocity field (added in quadrature), although this term could plausibly be as large as 5%. There is no allowance for bulk flow since we are explicitly trying to remove this by examining different reference frames. The average Hubble ratios are the weighted logarithmic averages, and the errors are those expected given the individual distance errors.

While this sample is too small to solve for a preferred reference frame at $4,000 \text{ km s}^{-1}$, we do see the insensitivity of the average Hubble ratio among the three frames because of the sampling over the sky. It is also apparent that χ^2 prefers the CMB frame to the Local Group or Abell Cluster frame, but again the numbers are small. Because these SBF distances appear to be extremely consistent and accurate, a larger sample observed by *HST* throughout the sky could give a precise measure of peculiar velocities; we discuss this issue further in §4.3. Our preferred value for H_0 is derived from the CMB frame since it has the lowest value of χ^2 : $H_0 = 82 \pm 8 \text{ km s}^{-1} \text{ Mpc}^{-1}$; the error is discussed in detail below.

3.2. The Far-Field H_0

The premise behind seeking the far-field is that the near-field may be strongly affected by random peculiar velocities or bulk flows. One measures distances in the near-field, but avoids using the corresponding near-field velocities by forming distance ratios between near and far objects, and then forming a Hubble ratio based purely on the far velocities. The classic example of this approach is using the distance to the nearby Virgo cluster, but adopting the velocity of the much more distant Coma cluster by finding the ratio of the Virgo to Coma distance from some form of relative distance estimator, such as the $D_n - \sigma$

method.

In the present case, the transference to the far field is somewhat less obvious as we are not making an explicit comparison of the four SBF BCG to, say, the most distant BCG in the Lauer & Postman (1994) sample at $15,000 \text{ km s}^{-1}$. Instead, we will implicitly compare the SBF BCG to the entire Lauer & Postman sample on the presumption that all BCG can be transferred to a common distance based on their observed velocities and a simple linear Hubble flow model. One can add a bulk flow to this model, but in the end, this makes little difference, as we discuss below.

The BCG $L_m - \alpha$ distance estimator presented in Lauer & Postman (1992, 1994) and Postman & Lauer (1995), indeed is based on comparing the physical properties of BCG after adopting a linear Hubble flow and an *ad hoc* H_0 . The $L_m - \alpha$ relation works by allowing L_m to be predicted based on α as measured at the metric radius r_m . The scatter in L_m is 0.24 mag, which translates into a typical distance error of $\sim 17\%$; this is larger than the error expected for a pure inverse-square distance estimator, as an error in the metric radius also implies an error in the apparent luminosity within the metric radius (Gunn & Oke 1975). The $L_m - \alpha$ relation is equivalent to assuming that BCG all have the same average enclosed surface brightness as a function of physical radius for a given value of α . Postman & Lauer (1995) showed that they could estimate BCG redshifts (that is a relative distance expressed as a velocity) to 17% accuracy from a surface brightness curve of growth by finding the angular aperture at which the enclosed surface brightness and α were consistent with the $L_m - \alpha$ relationship, then using the aperture size as a metric distance estimator.

Figure 9 shows the plot of estimated versus observed redshift presented by Postman & Lauer (1995). The estimated redshift results from calculating the velocity required to bring a given BCG onto the ridge line of the $L_m - \alpha$ relation. The scatter in z_e thus reflects the scatter of the BCG about the ridge line. Lauer & Postman (1994) showed that this scatter is strongly dominated by random photometric differences between the BCG rather than random peculiar velocities or velocity errors — photometric scatter is constant with redshift, as are the residuals about the $L_m - \alpha$ relationship, while the decreasing relative importance of random velocities with increasing Hubble velocity would cause the scatter to decline with red-

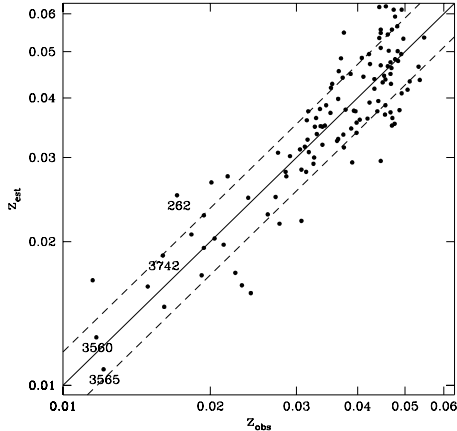


Fig. 9.— Redshifts of the BCG estimated from the $L_m - \alpha$ relationship versus observed redshifts are shown (see Postman & Lauer (1995)). Lines indicate equality of the two redshift measures and the $\pm 1\sigma$ errors in the estimated redshifts.

shift.

The estimated redshifts for the four SBF BCG (given in Table 3) imply the velocity scaling required to bring their photometric properties onto the $L_m - \alpha$ ridge line; Hubble ratios can then be calculated, based on the SBF distances. The implied far-field Hubble ratios are given in Table 3. Again, the average value is best estimated with a error-weighted logarithmic average of the ratios. The far-field Hubble constant implied is $H_0 = 89 \pm 10 \text{ km s}^{-1} \text{ Mpc}^{-1}$. The error will be discussed in detail in the next section, but in this case it is dominated by the BCG photometric scatter about the $L_m - \alpha$ relationship. In this context, it is worth noting that A262 is among the most deviant BCG with respect to its position in the $L_m - \alpha$ relationship, a conclusion echoed in the highly deviant Hubble ratio that it yields using its photometric redshift as the velocity (see the last column in Table 3). The χ^2 value for the far-field H_0 is also large. Deleting A262, yields a lower far-field $H_0 = 79 \pm 10 \text{ km s}^{-1} \text{ Mpc}^{-1}$. This value is consistent with the former value, but does suggest that a more complete sampling of the nearby BCG may be an attractive way to improve the accuracy of the BCG

far-field H_0 .

As the far-field H_0 does not explicitly depend on the velocities of the individual SBF BCG, it is explicitly independent of the velocity frame. There may be *implicit* dependences on frame, since different choices of Hubble velocity will affect the particular placement of any given BCG within the $L_m - \alpha$ relationship; however, such effects are tiny. For example, at $\alpha = 0.5$, the ridge line value of L_m varies by only 1% among the three frames. More to the point, the z_e varies by only 2% for A262, and less than 1% for the other BCG over the various frames. This result is not surprising, as any dipole pattern caused by a large bulk flow superimposed on the BCG recession velocities will integrate out of the $L_m - \alpha$ relationship because it is defined from the full sky.

A more relevant question is whether the nearby SBF BCG set may be offset from the more distant BCG by some global perturbation of the Hubble flow that is limited to within, say, 5,000 km s^{-1} or some other small fraction of the 15,000 km s^{-1} limit of the Abell Cluster sample. This was the sort of problem posed by Turner, Cen, & Ostriker (1992) and addressed by the Lauer & Postman (1992) BCG Hubble diagram. The linearity of the BCG Hubble diagram argued that $|\delta_H| < 0.07$ between 3,000 and 15,000 km s^{-1} . Further, Lauer & Postman (1992) showed that beyond 9,000 km s^{-1} , which includes the bulk of the BCG sample, $|\delta_H| \leq 0.02$ on radial shells of 3,000 km s^{-1} . In other words, there is no evidence that scatter in the $L_m - \alpha$ relationship or its ridge line is affected by any global variations in H_0 within 15,000 km s^{-1} . The $L_m - \alpha$ relationship is defined by the full BCG sample, unweighted by distance; the effective scale of the far-field BCG Hubble constant is just the average BCG recession velocity, or $\sim 11,000 \text{ km s}^{-1}$.

3.3. Errors in H_0

Both the “SBF-alone” and far-field H_0 values are affected by several random errors. The strong dependence of $\overline{M}_{I_{814}}$ on $(V - I)$ puts a premium on accurate colors. We do not have multiple ground observations of the BCG, but previous experience plus the quality of the standard star solutions argues that the error in $(V - I)$ is likely to be close to 0.012 mag. We also include a 10% uncertainty in E_{B-V} , and $\sim 20\%$ errors in the $(V - I)$ and \overline{I}_{814} k-corrections. The final net color error gives a typical ~ 0.09 mag error for estimating $\overline{M}_{I_{814}}$ from equation 2; this is added in quadrature to the measurement error in \overline{I}_{814} given in

Table 2 to give the total random distance error. Calculation of the Hubble ratios also includes a 184 km s^{-1} velocity error and 100 km s^{-1} peculiar velocity term for the SBF-alone measures, and a 17% redshift error for the Hubble diagram values, as noted above. The errors in the individual Hubble ratios given in Table 3 reflect the random error contributions only.

Important systematic errors include uncertainties in the F814W SBF calibration, the absolute zero point of the I_{KC} relationship on which it is based, and errors in the *HST* PSF. Scatter about the *HST* $\overline{M}_{I_{814}}$ versus $(V - I)$ relationship argues that the uncertainty in predicting $\overline{M}_{I_{814}}$, given perfect $(V - I)$, is $\sim 0.10 \text{ mag}$ (Ajhar et al. 1997). Tonry et al. (1997) give $\sim 0.07 \text{ mag}$ as the error in the I_{KC} SBF zero point, which itself is a composite of the statistical errors in the ground I_{KC} versus $(V - I)$ relationship plus uncertainties in the Cepheid calibration of the relationship. The systematic error associated with the PSF is 0.05 mag , as discussed in §2.4. If we add these errors in quadrature, we get a total systematic uncertainty of 0.13 mag in predicting distances.

We include no systematic error in velocity for H_0 estimated from the Hubble diagram. For the SBF-alone H_0 estimate, however, we do include an error for its relation to the true far-field value. Since the four SBF BCG are among the nearest of the Lauer & Postman (1994) sample, we take the net uncertainty in H_0 measured at $\sim 4,500 \text{ km s}^{-1}$ scales as 7%, given the variation of $\delta H \sim 0.07$, allowed out to $15,000 \text{ km s}^{-1}$ by the Lauer & Postman (1992) BCG Hubble diagram. In terms of velocity, this error corresponds to $\sim 300 \text{ km s}^{-1}$ at the SBF BCG distances, similar to plausible bulk flows on this scale, regardless of how the BCG sample the Lauer & Postman (1994) flow. The errors in the final average H_0 values given in Table 3 reflect the distance error, and except for the Hubble diagram solution, the 7% far-field error added in quadrature to the statistical error.

There are a number of paths for improving the present results. The Hubble diagram H_0 can best be refined by obtaining SBF distances to more nearby BCG. Refining the H_0 estimated solely from SBF distances, however, requires observation of more distant galaxies, as the present use of near-field velocities is an important uncertainty. Improving the F814W SBF calibration will also be useful. Fortunately, *HST* SBF observations for the nearest galaxies can generally be done within an orbit, and in many cases may be made from images obtained for other purposes, as was the

case for the Ajhar et al. (1997) sample. Because this calibration may improve, we have attempted to make the path from \overline{T}_{814} to distances readily visible. Revised values of H_0 can thus be quickly derived when better data become available.

4. Discussion

4.1. Comparison of Recent H_0 Measurements

The present H_0 values are somewhat larger than many recent H_0 measurements based on calibration of Hubble diagrams of a variety of distance estimators, but they are consistent with the higher of the comparisons. Giovanelli et al. (1997) find $H_0 = 69 \pm 5 \text{ km s}^{-1} \text{ Mpc}^{-1}$, using Cepheid distances to 12 galaxies, which were used to calibrate a composite Tully-Fisher relationship based on 24 clusters of galaxies within $9,000 \text{ km s}^{-1}$. As do we, Giovanelli et al. emphasize their independence from the classic Virgo/Coma distance ratio approach. Giovanelli et al. did not show a Hubble diagram, nor list their clusters, but from their description of the cluster distribution, we estimate that the effective depth of their H_0 determination is $\sim 6,000 \text{ km s}^{-1}$. Calibration of the Tully-Fisher relationship has been a major goal of the *HST* Cepheid key project as well (Freedman et al. 1994). Mould et al. (1995) find $H_0 = 82 \pm 11 \text{ km s}^{-1} \text{ Mpc}^{-1}$, based on a Tully-Fisher calibration that reaches beyond $4,000 \text{ km s}^{-1}$, but that also depends heavily on the Virgo cluster sample. Freedman (1997) gives $H_0 = 73 \pm 8 \text{ km s}^{-1} \text{ Mpc}^{-1}$, as a provisional summary of the key project work to date.

Supernovae also are providing excellent probes of the Hubble flow. Riess, Press, & Kirshner (1996) present a Hubble diagram based on their light curve-shape method applied to 20 SN Ia's; using three Cepheid calibrators, they conclude $H_0 = 64 \pm 6 \text{ km s}^{-1} \text{ Mpc}^{-1}$ on $\sim 7,000 \text{ km s}^{-1}$ scales. Hamuy et al. (1996) find $H_0 = 63 \pm 4 \text{ km s}^{-1} \text{ Mpc}^{-1}$, an essentially identical result, using their Δm_{15} decay rate estimator applied to 29 SN Ia with an effective depth of $\sim 12,000 \text{ km s}^{-1}$. Proper use of SN Ia as distance estimators remains controversial, however, with significant disagreement on how the light curve decay rate relates to the SN Ia peak luminosity. Sandage et al. (1996), for example, emphasize a Hubble diagram approach as well, using SN Ia's, and conclude $H_0 = 57 \pm 4 \text{ km s}^{-1} \text{ Mpc}^{-1}$. This value, while consistent with those of Riess, Press, & Kirshner (1996) and Hamuy et al. (1996), argues for H_0 near the lower ends of their error bars, rather

than the upper ends, as would be more consistent with the Tully-Fisher results cited above and the present BCG results. Kennicutt, Freedman, & Mould (1995) present a figure showing large dispersion in H_0 values calculated from SN Ia alone over the last few years; agreement on how to calibrate the SN Ia distance scale remains work for the future.

There is an abundance of other recent measurements of H_0 that we could cite, but as many of them are based heavily or exclusively on the Virgo or Coma clusters, we find them less attractive than methods featuring rich sampling of the Hubble flow. It is also worth noting that while we are comparing H_0 estimates that all depend on the *HST* Cepheid calibration work, different methods make use of different calibrators, which may account for a portion of the variance in H_0 among authors. At this writing, Feast & Whitelock (1997) are arguing that the Cepheid scale, itself, should be revised based on *Hipparcos* parallax measurements. If so, then the Tonry et al. (1997) and Ajhar et al. (1997) SBF zero points will need revision.

Two promising alternative approaches for measuring H_0 , which are completely independent of local calibration, are gravitational lens induced time delay observations and measurement of the Sunyaev-Zel'dovich (SZ) effect for $z \gg 0.05$ clusters. As Freedman (1997) summarizes, however, measurements of the SZ effect are neither accurate nor consistent enough at this time to provide an H_0 that challenges the more local measures. Gravitational lenses also have the potential to produce a far-field H_0 that steps over all the distance-ladder problems that bedevil more traditional methods; however, detailed mass distributions of the lenses are required, which presently limits their accuracy. Kundić et al. (1997) find $H_0 = 64 \pm 13 \text{ km s}^{-1} \text{ Mpc}^{-1}$, based on the observed time delay between the two QSO images in the classic 0957 + 561 lens at $z = 0.36$. In contrast, Schechter et al. (1997) present time delays and mass models for the lens PG 1115 + 080 that favor $H_0 = 42$, although they also present a model that gives $H_0 = 64$. It is thus difficult to make a strong case at present that gravitational lenses, which probe the Hubble flow on extremely large scales, are yielding consistent H_0 values significantly smaller than the $z \leq 0.05$ measurements.

4.2. Is the BCG Far-Field Far Enough?

Observational evidence suggests that the far-field has been reached. While the sampling of the Hubble flow remains sparse beyond $15,000 \text{ km s}^{-1}$, the limiting radius of Lauer & Postman (1992), the SN Ia Hubble diagrams of Riess, Press, & Kirshner (1996) and Hamuy et al. (1996) are consistent with linear flows out to $\sim 30,000 \text{ km s}^{-1}$. Going to cosmological distances, Kim et al. (1997) use SN Ia to constrain δ_H by comparing 28 SN with $0.35 < z < 0.65$ to 18 SN of the Hamuy et al. (1996) sample. The motivation for developing such SN Hubble diagrams is to measure Ω_M and Λ ; such cosmological tests presume an unbiased local Hubble flow as a point of departure. On the other hand, with assumed Ω_M and Λ , one can test for significant δ_H over extremely large scales. For $\Omega_M \leq 1$, Kim et al. find $\delta_H < 0.05$ (1σ), or $\delta_H < 0.1$ (95% confidence). For $\Omega_M \ll 1$ with $\Lambda = 0$, or $\Omega + \Lambda = 1$, one can get $\delta_H \lesssim -0.1$, corresponding to global H_0 actually *larger* than the local value.

Going out far enough to measure the unbiased H_0 means reaching the scale on which mass density fluctuations no longer generate significant velocity perturbations of the Hubble flow. The most important bias to consider for a full-sky determination of H_0 is the global radial retardation or acceleration of the Hubble flow that occurs within significant mass over- or under-densities. The possibility that we are within a large bubble of lower than cosmic density, for example has been proposed as a way of reconciling apparently high H_0 values measured nearby, with the estimated age of the universe, and the often-cited concern (e.g. Bartlett et al. 1995) that extremely far-field H_0 measures such as those from the SZ effect or lenses are lower than the more local measures (although, as noted above, the case for this is weak). Berschinger (1985) and Ryden (1994) present analytic treatments of how voids grow with time. The voids effectively expand faster than the cosmic scale factor; observers well inside the voids would see linear, if spuriously rapid Hubble flows. Shi, Widrow, & Dursi (1996) in general find $\delta_H \sim -0.6\delta M/M$, where $\delta M/M$ is the relative mass-deficit of the void.

When limited to popular initial power-spectra, however, one predicts only small δ_H over the large volumes sampled by BCG and SN Ia. Turner, Cen, & Ostriker (1992), for example, confined their analysis to very modest scales compared to the Hubble dia-

grams now available. The large variations in δ_H that they observed under CDM and PIB power-spectra occurred for volumes limited to $3,000 \text{ km s}^{-1}$. For volumes limited to $6,000 \text{ km s}^{-1}$, they found $\langle \delta_H \rangle < 0.05$, depending on the power-spectrum. Shi, Widrow, & Dursi (1996) likewise conclude that $\langle \delta_H \rangle \sim 0.05$ on $15,000 \text{ km s}^{-1}$ scales with “reasonable” models of galaxy and structure formation.

The question of whether or not we have gone out far enough in measuring the Hubble flow thus remains an issue only if there is significantly more power in mass-fluctuations on large scales than would be expected under standard theories. In this context, we can posit that the 689 km s^{-1} bulk flow observed by Lauer & Postman (1994) in the volume limited to $15,000 \text{ km s}^{-1}$ is indeed evidence for such power on large scales. Strauss et al. (1995), and Feldman & Watkins (1994) both find the Abell cluster bulk flow to be incompatible at $\sim 95\%$ confidence with all standard models of galaxy formation considered. Tegmark, Bunn, & Hu (1994) further argue that the Lauer-Postman bulk flow is not compatible with degree-scale measurements of the CMB anisotropy power-spectrum. Even so, however, Shi, Widrow, & Dursi (1996), taking the Harrison-Zel’dovich power spectrum shape and normalization parameters that best fit the Lauer-Postman flow (see Jaffe & Kaiser 1995), still find that only modest $\delta_H = 0.05$ would be expected. At the same time, Shi, Widrow, & Dursi show that the range of power spectra considered by Jaffe & Kaiser to fit the Lauer-Postman bulk flow would admit δ_H as large as 0.12 in the limiting extreme case.

Of course, power-spectra give only a statistical expectation for the local distribution of matter. One remains free to argue that we are within a local density anomaly that exceeds the $\pm 1\sigma$ fluctuations at some level. In this case, Shi, Widrow, & Dursi (1996) discuss the CMB dipole and quadrupole anisotropies that would be observed within the anomaly and conclude that they would put strong constraints on the allowed geometry of the local density fluctuation (see also Tomita 1996). We conclude that while one can construct models of the universe for which the far-field remains at distances well in excess of those explored here, they are extremely disfavored by what we know of the power-spectrum of initial mass fluctuations in the universe.

4.3. The Abell Cluster Bulk Flow

The accuracy of these SBF distances offers the means to test the validity of different reference frames, although we cannot legitimately solve for an independent, best-fit reference frame with only four points. As described in section §3.1, we consider three reference frames: CMB (for obvious reasons), Local Group (since for smooth flows this has zero dipole locally), and Abell Cluster (AC) frame following the Lauer & Postman (1994) bulk flow. Although we tried to remove all systematic, common contributors to the errors in the SBF distances when calculating χ^2 for our H_0 estimates, we find that χ^2/N in Table 3 ($N = 3$) has a value of 0.3 for the CMB frame. This may indicate that we have overestimated our errors, since such a value or lower will occur only 18% of the time by chance, so we bear in mind that all the true χ^2 values may be larger than what is listed in Table 3. At the same time, it seems unlikely that our random errors could be overestimated by a factor of almost 2, necessary to raise χ^2/N in the CMB frame to unity, so at least some of the concordance of results in this frame surely is coincidence. Taking the numbers at face value, the probability that χ^2/N is at least as large as 1.2 (the LG value) is 0.31, and the probability that χ^2/N is at least as large as 2.4 (the AC frame value) is 0.07. Thus our observations offer the most support for these four clusters being at rest in the CMB frame.

The very small number of SBF distances does not permit us say whether this rejects the AC frame or not, since the AC frame was chosen to minimize the scatter of the $L_m - \alpha$ relationship for 119 clusters at distances much greater than our sample here. Additionally, we are guessing at a random velocity component of 209 km s^{-1} (100 and 184 in quadrature). If the random velocity is as large as 500 km s^{-1} the AC frame will have unity χ^2/N (0.1 in the CMB frame).

It is clear that A262 is problematic for $L_m - \alpha$ as seen in Figures 1, 2, and 9; it has a very low surface brightness and hence its distance is estimated to be large. Likewise, the SBF and $L_m - \alpha$ distances are consistent within the errors for A3560, A3565, and A3742, but there is a 3σ inconsistency with A262. The cosmic scatter in the $L_m - \alpha$ is clearly related to intrinsic variations in metric surface brightness among the BCG. Lauer & Postman (1994) note that this scatter greatly dominates any variation in L_m due to peculiar velocity, but rely the assumption that in-

TABLE 3
HUBBLE RATIOS AND H_0

Abell	D Mpc	z_{est}	H_0 (CMB)	H_0 (LG)	H_0 (AC)	H_0 (BCG)
262	57 ± 5	0.0250	82 ± 8	90 ± 9	94 ± 9	132 ± 25
3560	47 ± 3	0.0126	86 ± 7	75 ± 7	72 ± 6	81 ± 15
3565	49 ± 3	0.0108	83 ± 6	73 ± 6	70 ± 6	66 ± 12
3742	60 ± 3	0.0187	78 ± 6	80 ± 6	79 ± 6	94 ± 17
Averages			82 ± 8	79 ± 8	78 ± 8	89 ± 10
χ^2/N			0.3	1.2	2.4	2.6

NOTE.—The third column is the redshift estimated from the BCG $L_m - \alpha$ relationship (see Postman & Lauer 1995). Hubble ratios are in $\text{km s}^{-1} \text{Mpc}^{-1}$. The “Averages” line gives the logarithmic average of the individual ratios, with error bars reflecting all systematic errors (see text). χ^2/N is calculated using errors without common, systematic contributions, and gives an indication of the internal consistency of the ratios.

trinsic variations in BCG surface brightness are not correlated over large angles and will average out of a large sample. In the case of A262, however, the AC frame does partially compensate for the discrepancy between its $L_m - \alpha$ distance and its redshift. The rms scatter in the $L_m - \alpha$ relationship for just these four clusters is 0.41 mag in the CMB frame, but only 0.27 mag in the Abell Cluster frame. If we delete A262 the rms $L_m - \alpha$ residuals drop to 0.29 mag (CMB), and 0.20 mag (AC). In their analysis Lauer & Postman tried deleting outliers (such as A262) and found the AC frame to be quite stable, so this is not the whole story. Nevertheless it seems clear that a larger sample of SBF distances could not only provide a very accurate reference frame and random velocity amplitude, but also allow us to understand why the Lauer & Postman sample and the $L_m - \alpha$ relation point to the AC frame.

4.4. The Distance to the Virgo Cluster

Lauer & Postman (1992) originally attempted to calibrate the BCG Hubble diagram on the presumption that NGC 4472, the Virgo cluster BCG, was typi-

cal. Adopting a 14.4 Mpc distance to NGC 4472, they found $H_0 = 77 \pm 8 \text{ km s}^{-1} \text{Mpc}^{-1}$; however, if they adopted the Sandage & Tammann (1990) 21.9 Mpc Virgo distance for NGC 4472, $H_0 = 51 \pm 5$ would be implied. Our present results for H_0 are essentially identical to that obtained with the short distance to NGC 4472, and are significantly different from that obtained from the with distance, arguing that the distance to the Virgo core is indeed close to the shorter value. If NGC 4472 were at the distance of 21.9 Mpc, then it would be among the brightest of the Lauer & Postman (1994) sample, deviating from the $L_m - \alpha$ ridge line by more than 2σ . Of course, one could question this conclusion by challenging the SBF calibration, since it is already known that SBF distances imply a short distance to Virgo (Tonry et al. 1997); however, this still remains as an important consistency check. The relative distances inferred from BCG are consistent with SBF distances.

5. Conclusion

We have used *HST* to obtain SBF distances to four BCG beyond 4,000 km s^{-1} to calibrate the Lauer

& Postman (1992) BCG Hubble diagram, producing an estimate of the global value of H_0 valid on $\sim 11,000 \text{ km s}^{-1}$ scales. This method gives $H_0 = 89 \pm 10 \text{ km s}^{-1} \text{ Mpc}^{-1}$, and is based on the full Lauer & Postman (1994) 15,000 km s^{-1} volume limited BCG sample. As such, the result is independent of Virgo or Coma cluster distances and membership issues, as well as the recession velocities of the four BCG studied. The large error reflects the photometric scatter about the $L_m - \alpha$ ridge line, which was used to transfer the BCG Hubble diagram to the SBF distance scale. As more BCG are observed with *HST*, the formal errors in this far-field H_0 should decrease.

Our review of the present understanding of the formation of large scale structure argues that we are likely to have fairly sampled the far-field. Even theories with enough power on large spatial scales to generate bulk flows as large as those observed by Lauer & Postman (1994) are unlikely to have deviations outside of $|\delta_H| \lesssim 0.05$ for the volume sampled by the BCG Hubble diagram. In contrast, the compatibility of our results with those based on more nearby objects argues that there is little effect on H_0 and the depth of the measurements. Going to the far-field most likely removes a source of uncertainty, rather than correcting for a systematic error. Indeed we find $H_0 = 82 \pm 8 \text{ km s}^{-1} \text{ Mpc}^{-1}$ just from Hubble ratios based on the SBF distances and observed recession velocities to the four SBF-calibrated BCG at $\sim 4,000 \text{ km s}^{-1}$ alone, a result consistent with our far-field result.

The present H_0 rests on calibration of the SBF method and an understanding of its systematic effects. At the fundamental level, we are tied to the nearby Cepheid calibrators. Changes in the Cepheid scale will propagate to the present results through the Tonry et al. and Ajhar et al. calibrations. As noted in the introduction, Tonry et al. (1997) SBF calibration is tied to seven spiral galaxies with Cepheid distances. Further, Tonry et al. have observed enough galaxies to perform an exhaustive series of tests, finding no systematic offsets between SBF observations of bulges and elliptical galaxies. A weaker link is transferring the ground I_{KC} method to the WFPC2 F814W filter, a task accomplished by Ajhar et al. (1997); we will attempt to refine this calibration as more nearby systems are observed with *HST*. We conclude that the major uncertainties in the distance scale are those close to home rather than far away.

We thank Guy Worthey and Barbara Ryden for helpful discussions, and John Blakeslee for the photometry of A262. This research was supported in part by *HST* GO analysis funds provided through STScI grant GO-05910.03-94A.

REFERENCES

- Ajhar, E. A., Lauer, T. R., Tonry, J. L., Blakeslee, J. B., Dressler, A., Holtzman, J. A., & Postman, M. 1997, *AJ*, 114, 626
- Bartlett, J. G., Blanchard, A., Silk, J., & Turner, M. S. 1995, *Science*, 267, 980
- Baum, W. A., Hammergren, M., Thomsen, B., Groth, E. J., Faber, S. M., Grillmair, C. J., & Ajhar, E. A. 1997, *AJ*, 113, 1483
- Bertschinger, E. 1984, *ApJS*, 58, 1
- Blakeslee, J. P., & Tonry, J. L. 1996, *ApJ*, 465, L19
- Burstein, D., & Heiles, C. 1984, *ApJS*, 54, 33
- Feast, M. W., & Whitelock, P. A. 1997, preprint, astro-ph/9706097
- Feldman, H. A., & Watkins, R. 1994, *ApJ*, 430, L17
- Freedman, W. L. et al. 1994, *Nature*, 371, 757
- Freedman, W. L. 1997, in 18th Texas Symposium, eds. Olinto, A., Frieman, J., & Schramm, D. (World Scientific)
- Giovanelli, R., Haynes, M. P., da Costa, L. N., Freudling, W., Salzer, J. J., & Wegner, G. 1997, *ApJ*, 477, L1
- Gunn, J. E., Oke, J. B. 1975, *ApJ*, 195, 255
- Hamuy, M., Phillips, M. M., Suntzeff, N. B., Schommer, R. A., Maza, J., & Avilés, R. 1996, *AJ*, 112, 2398
- Holtzman, J. A., Burrows, C. J., Casertano, S., Hester, J. J., Trauger, J. T., Watson, A. M., Worthey, G. 1995a, *PASP*, 107, 1065
- Hoessel, J. G. 1980, *ApJ*, 241, 493
- Holtzman, J. A., et al. 1995b, *PASP*, 107, 156
- Jacoby, G. H., Branch, D., Ciardullo, R., Davies, R. L., Harris, W. E., Pierce, M. J., Pritchet, C. J., Tonry, J. L., & Welch, D. L. 1992, *PASP*, 104, 599
- Jaffe, A. H., & Kaiser, N. 1995, 455, 26
- Kennicutt, R. C., Freedman, W. L., & Mould, J. R., 1995, *AJ*, 110, 1476
- Kim, A. G. et al. 1997, *ApJ*, 476, L63

Kundić, T. et al. 1997, ApJ, 482, 75

Lauer, T. R., & Postman, M. 1992, ApJ, 400, L47

Lauer, T. R., & Postman, M. 1994, ApJ, 425, 418

Mould, J. et al. 1995, ApJ, 449, 413

Postman, M., & Lauer, T. R. 1995, ApJ, 440, 28

Riess, A. G., Press, W. H., Kirshner, R. P. 1996, ApJ, 473, 88

Ryden, B. S. 1995, ApJ, 452, 25

Sandage, A. 1972, ApJ, 178, 1

Sandage, A. & Hardy, E. 1973, ApJ, 183, 743

Sandage, A., & Tammann, G. A. 1990, ApJ, 365, 1

Sandage, A., Saha, A., Tammann, G. A., Labhardt, L., Panagia, N., & Macchetto, F. D. 1996, ApJ, 460, L15

Schechter, P. L., Mateo, M., & Saha, A. 1993, PASP, 105, 1342

Schechter, P. L. et al. 1997, ApJ, 475, L85

Schmidt, B. P., Kirshner, R. P., Eastman, R. G., Phillips, M. M., Suntzeff, N. B., Hamuy, M., Maza, J., & Aviles, R. 1994, ApJ, 432, 42

Shi, X., Widrow, L. M., & Dursi, L. J. 1996, MNRAS, 281, 565

Strauss, M. A., Cen, R., Ostriker, J. P., Lauer, T. R., & Postman, M. 1995, ApJ, 444, 507

Tammann, G. A. 1992, Phys. Scr, T43, 31

Tegmark, M., Bunn, E. F., & Hu, W. 1994, ApJ, 434, 1

Tomita, K. 1996, ApJ, 461, 507

Tonry, J. L., Ajhar, E. A., & Luppino, G. A. 1990, AJ, 100, 1416

Tonry, J. L., Blakeslee, J. B., Ajhar, E. A., & Dressler, A. 1997, ApJ, 475, 399

Tonry, J. L., & Schneider, D. P. 1988, AJ, 96, 807

Turner, E. L., Cen, R., & Ostriker, J. P. 1992, AJ, 103, 1427

Whitmore, B. C., Sparks, W. B., Lucas, R. A., Macchetto, F. D., & Biretta, J. A. 1995, ApJ, 454, L73

Worthey, G. 1993a, ApJ, 409, 530

Worthey, G. 1993b, ApJ, 418, 947

This 2-column preprint was prepared with the AAS L^AT_EX macros v4.0.

This figure "figure3.jpg" is available in "jpg" format from:

<http://arxiv.org/ps/astro-ph/9708252v1>

This figure "figure4.jpg" is available in "jpg" format from:

<http://arxiv.org/ps/astro-ph/9708252v1>

This figure "figure5.jpg" is available in "jpg" format from:

<http://arxiv.org/ps/astro-ph/9708252v1>

This figure "figure6.jpg" is available in "jpg" format from:

<http://arxiv.org/ps/astro-ph/9708252v1>